Electrochemical Materials and Technologies

FOCUS REVIEW

Electrochemical Materials and Technologies

eISSN: 2949-0561

Cite this: Electrochem. Mater. Technol. 1 (2022) 20221004

Layered and hexagonal perovskites as novel classes of proton-conducting solid electrolytes. A focus review

Natalia Tarasova [ab]*, Irina Animitsa [ab], Anzhelika Galisheva [ab], Dmitry Medvedev [ab]

Received: 15 September 2022
Accepted: 28 September 2022

DOI: 10.15826/elmattech.2022.1.004

Solid oxide electrolytes have attracted significant attention due to their possible applications in energy conversion devices, including solid oxide fuel cells (SOFCs) and electrolysis cells (SOECs). Although a large amount of data has been accumulated to date, the design of new representatives of ionic electrolytes is of unquenchable interest. In this paper, a review of the new classes of proton-conducting solid electrolytes is provided. The physicochemical and transport properties of layered perovskites ($BaNdInO_4$, $BaNdScO_4$, $SrLaInO_4$, $BaLaInO_4$) and hexagonal perovskites ($Ba_7Nb_4MoO_{20}$, $Ba_5Er_2Al_2ZrO_{13}$ and $Ba_5In_2Al_2ZrO_{13}$) were analyzed and summarized. Based on the performed analysis, the most promising compositions among the considered phases were identified and the effective approaches aimed at improving their functional characteristics were provided.

keywords: layered perovskite, Ruddlesden-Popper structure, hexagonal perovskite, proton conductivity, SOFCs, SOECs

1. Introduction

Today, hydrogen energy is one of the most developing areas of clean energy due to various advantages of hydrogen compared to traditional fossil fuels [1]. To ensure the technological processes in this area, it is necessary to develop systems for the production, purification, storage of hydrogen and the devices for electricity generation. One of such devices is solid oxide fuel cells (SOFCs). Their development on a commercial scale requires the selection of different types of high-effective materials, including electrodes [2–9] and electrolytes [10–12]. Most of these materials have perovskite structure.

However, during the last several years, the proton-conducting electrolyte families have been replenished with members of the new structural classes, named layered perovskites and hexagonal perovskites. Both are promising, and both can lead to the creation of novel advanced proton-conducting ceramic materials for energy conversion technologies.

2. Layered perovskites

The derivative structures from an ordinary perovskite were described by S.N. Ruddlesden and P. Popper in 1957 [13]. In this structure with a general formula of $AA'BX_4$, the [A/A'BX$_3$] perovskite layers were divided by the [A/A'X] rock salt layers. Over the past sixty years, the layered perovskites have been extensively investigated as superconductors

a: Institute of High-Temperature Electrochemistry, Ekaterinburg 620009, Russia
b: Ural Federal University, Ekaterinburg 620009, Russia

* Corresponding author: natalia.tarasova@urfu.ru

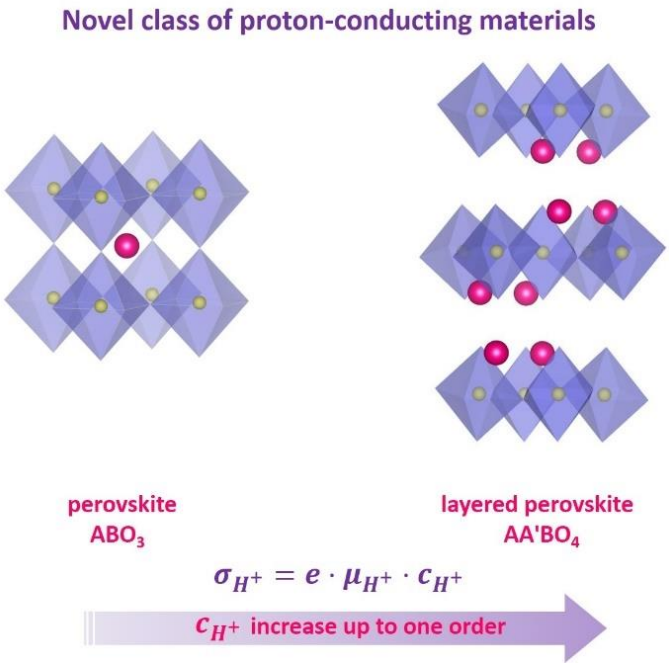

Figure 1 The crystal structure of perovskite (left image) and layered perovskite (right image).

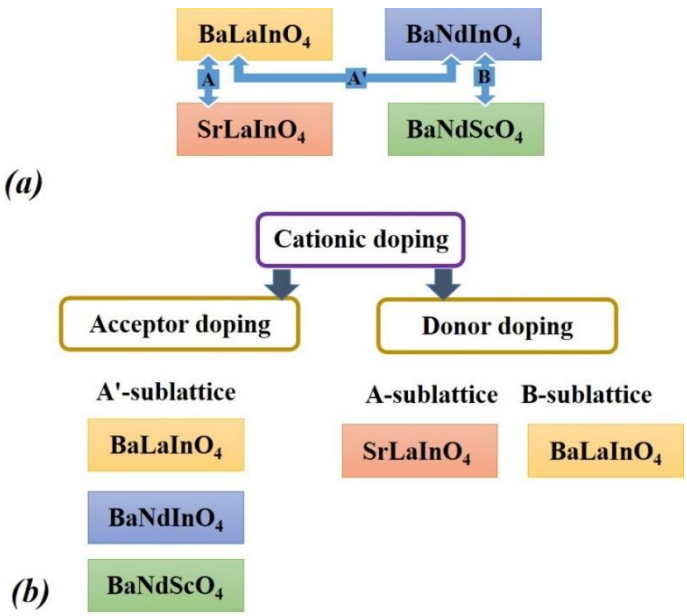

Figure 2 The schemes demonstrating the possibility of change of all cations in $AA'BO_4$ (a) and the application of cationic doping for the improvement of proton conductivity (b).

[14–18], magnetic [19–22] and electrode materials [23–32], phosphors [33–35] and photocatalysts [36–38]. However, the first articles which considered layered perovskites as proton electrolytic materials were published only in 2015 [39] (Figure 1).

Proton-conducting layered perovskites can be described by a general $AA'BO_4$ formula, where A is the rare earth metal, A′ is the lanthanum or lanthanide, B is the trivalent p-element.

Figure 2a demonstrates the possibility of change of all cations in $AA'BO_4$. The materials based on $BaLaInO_4$, $SrLaInO_4$, $BaNdInO_4$, and $BaNdScO_4$ can exhibit a significant level (up to almost 100%) of protonic transport [40–52]. However, the difference in nature of the cations determines the corresponding differences in the crystal structure of the materials. The compositions of $BaLaInO_4$ and $SrLaInO_4$ are described in an orthorhombic symmetry with the space group *Pbca*, while the compositions of $BaNdScO_4$ and $BaNdInO_4$ belong to *Cmcm* (orthorhombic symmetry) and $P2_1/c$ (monoclinic symmetry) space group, respectively. It is reasonable to compare the temperature dependencies of the proton conductivity for these matrix (undoped) compositions. However, this is not possible due to a lack of the literature data.

The most common way to improve transport properties for proton-conducting $AA'BO_4$ layered perovskites is to dope them in the A'-sublattice, particularly with calcium ions (Figure 2b). The compositions of $BaNd_{1-x}Ca_xInO_{4-0.5x}$ [40] and $BaNd_{1-x}Ca_xScO_{4-0.5x}$ [41] (where x = 0.1 and 0.2), as well as the $BaLa_{0.9}Ca_{0.1}InO_{3.95}$ composition [43], were obtained. The quasi-chemical equation of acceptor doping can be described as:

$$2MO \xrightarrow{Ln_2O_3} 2M'_{Ln} + 2O_O^{\times} + V_O^{\bullet\bullet} \quad (1)$$

An increase in the calcium-content in $BaNd_{1-x}Ca_xInO_{4-0.5x}$ led to a decrease in the unit cell volume from 441.54 Å for $BaNdInO_4$ to 438.21 Å for $BaNd_{0.8}Ca_{0.2}InO_{3.9}$.

The temperature dependencies of conductivity were obtained using impedance spectroscopy method in the various atmospheres (dry air, wet air, and nitrogen). The gas drying was performed using $CaSO_4$, the gas bubbling through H_2O was used for the humidification. The fitting of impedance spectra showed that they were composed of two semicircles at low temperatures (below 300 °C), and the bulk component of the resistance could not be used for the conductivity calculation. In the dry air atmosphere, the calcium-doping led to the increase of the total conductivity values by up to ~2 orders of magnitude. The most conductive composition was $BaNd_{0.8}Ca_{0.2}InO_{3.9}$. It should be noted that the doping led to a decrease in the energy activation from 0.78 eV for $BaNdInO_4$ to 0.71 eV for $BaNd_{0.8}Ca_{0.2}InO_{3.9}$ at low temperatures. The formation of oxygen vacancies during acceptor doping was the reason for this significant decrease.

The conductivity investigations in wet air were performed for the most-conductive composition, i.e.

$BaNd_{0.8}Ca_{0.2}InO_{3.9}$. It was shown that the activation energy was 0.68 eV in the wet air and 0.64 eV in the wet nitrogen, which was close to the values of the proton transport in the non-layered perovskites [53, 54]. The conductivity values obtained in wet nitrogen were lower than in the wet air, which indicated the mixed ionic-hole nature of conductivity. The proton transport numbers increased from 0.41 to 0.57 over a temperature range of 250–475 °C. That is, the $BaNd_{0.8}Ca_{0.2}InO_{3.9}$ composition demonstrated mixed protonic-hole conductivity in wet air atmosphere with a value of $4\cdot10^{-4}$ S/cm at 475 °C, and the contribution of proton transport was about 57% at the same temperature. The thermogravimetric investigations showed that the maximum concentration of protonic defects at 500 °C was about 2.2 mol %, which corresponded to the 1.1 mol water per formula unit. However, the A-cation exsolution processes were observed during the annealing of this composition at 500 °C in a wet atmosphere for a week. It indicated poor chemical stability of this type of materials [40].

For the solid solution of $BaNd_{1-x}Ca_xScO_{4-0.5x}$, an increase in the calcium-content led to a decrease in the unit cell volume, as well [41]. However, the a-lattice parameter increased, opposite to the decreasing values of b- and c-parameters. The electrical conductivity measurements were performed by a DC 4-probe method in dry ($pH_2O \leq 1.2\cdot10^{-16}$ atm) and wet ($pH_2O = 2.3\cdot10^{-2}$ atm) atmospheres, as well as in the static air. The measurements of total conductivity values in the static air identified the $BaNd_{0.8}Ca_{0.2}ScO_{3.9}$ composition as the most conductive. The total conductivity values were found to be equal to $3.1\cdot10^{-4}$ S/cm, $1.1\cdot10^{-2}$ S/cm and $1.2\cdot10^{-2}$ S/cm at 800 °C for compositions with $x = 0$, $x = 0.1$ and $x = 0.2$, respectively. The use of N_2/H_2 and N_2/O_2 gas mixtures allowed for the identification of nature of electrical conductivity. It was shown that both matrix and calcium-doped compositions were characterized by a mixed ionic-hole type of conductivity in air ($pO_2 = 0.21$ atm). The oxygen-ionic conductivity was defined as conductivity measured in the dry atmosphere under low oxygen partial pressure ($pO_2 < 10^{-8}$ atm). The proton conductivity values were obtained as a difference between the ionic conductivity values obtained in wet and dry atmospheres at the same temperature. The proton conductivity for the calcium-doped composition was higher than that of the matrix composition by up to ~ 1.5 orders of magnitude at 600 °C. The proton transport numbers were estimated to be 0.88 and 0.62 for $BaNdScO_4$ and $BaNd_{0.8}Ca_{0.2}ScO_{3.9}$ at 700 °C, respectively. We can assume that the transport numbers at lower temperatures would be higher, but the data for the composition $BaNd_{0.8}Ca_{0.2}ScO_{3.9}$ were not provided. The increase in the proton mobility by 2.2 times, according to the calculations from the Arrhenius plots [41], was the reason for the increase in the proton conductivity for the doped composition. However, the proton concentration in the structure was not defined.

In contrast, for the calcium-doped $BaLaInO_4$, the values of water uptake, as well as the proton conductivity and proton transport numbers, were calculated in [43]. The introduction of calcium-ions into the lanthanum-sublattice led to an increase in the unit cell volume from 450.19 Å for $BaLaInO_4$ to 451.22 Å for $BaLa_{0.9}Ca_{0.1}InO_{3.95}$. This pattern is opposite to dependencies observed for the calcium-doped $BaNdInO_4$ and $BaNdScO_4$ counterparts and can be explained by differences in their crystal lattice symmetry. The conductivity values were obtained using impedance spectroscopy measurements in dry air ($pH_2O = 3.5\cdot10^{-5}$ atm), wet air ($pH_2O = 2\cdot10^{-2}$ atm), and Ar. For both undoped and doped compositions, the Nyquist plots contained one semicircle, starting from the coordinate origin in the entire investigated temperature range (300–900 °C); this allowed for the bulk resistance values to be obtained for calculations of partial conductivity values. The proton conductivity values for $BaLaInO_4$ and $BaLa_{0.9}Ca_{0.1}InO_{3.95}$ were calculated as a difference between conductivity values obtained in wet Ar and dry Ar (oxygen-ionic conductivity) at the same temperature. It was shown that calcium-doping led to an increase in the proton conductivity by up to ~1.2 orders of magnitude. According to the thermogravimetric measurements, the calcium-doping also led to an increase in the water uptake from 0.6 mol H_2O per formula unit for the basic composition to 0.7 mol for the Ca-doped sample, i.e. the proton concentration increased. This indicated that the increase in the proton conductivity was due to a higher concentration of proton charge carriers in the structure. It should be noted that the proton transport numbers were approximately 0.9 for both undoped and doped compositions, which was sufficiently higher compared to those obtained for $BaNdIn(Sc)O_4$ and their calcium-doped analogs. The high proton transport numbers can be considered as an advantage for the compositions based on $BaLaInO_4$ in comparison with the compositions based on $BaNdInO_4$ and $BaNdScO_4$, despite the lower proton conductivity values (Figure 3).

The improvement of transport properties of $AA'BO_4$ layered perovskites was also verified by a donor-type doping of A- and B- sublattices. This type of doping

led to the formation of interstitial oxygen defects in the interlayer space of crystal lattice:

$$M_2O_3 \xrightarrow{2AO} 2M_A^{\bullet} + 2O_O^{\times} + O_i'' \quad (2)$$

$$2MO_2 \xrightarrow{B_2O_3} 2M_B^{\bullet} + 3O_O^{\times} + O_i'' \quad (3)$$

The presence of protons in the donor-doped $SrLaInO_4$ structure was proven by the neutron powder diffraction analysis [42]. It was shown that the formation of $Ba_xSr_{0.8-x}La_{1.2}InO_{4+d}$ solid solutions was accompanied by an increase in the unit cell volume from 432.42 Å for $SrLaInO_4$ to 437.12 Å for the composition with $x = 0.3$.

The electrical conductivity measurements were performed only in ambient air without any control of water vapor partial pressure; therefore, the proton conductivity could not be calculated. However, the donor doping of La-sublattice of $SrLaInO_4$ is a promising way of improving transport properties. The conductivity values of the composition with $x = 0.3$ is higher than that of the undoped $SrLaInO_4$ by approximately 0.25 orders of magnitude.

Systematic investigations on the influence of the size and concentration of dopant were performed for $BaLaInO_4$ composition [43–52]. Apart from Ca^{2+}-ions, Sr^{2+}- and Ba^{2+}-ions were used as the acceptor dopants introduced in the La^{3+}-sublattice of $BaLaInO_4$ [43, 45]. The ions Ti^{4+}, Zr^{4+} and Nb^{5+} were used for the donor doping of the In^{3+}-sublattice [44, 46, 48, 49]. All doped compositions based on $BaLaInO_4$ were characterized by the *Pbca* space group. Both type of doping (acceptor and donor) led to an increase in the unit cell volume due to the increase in both the a-lattice parameter and interlayer space between the perovskite blocks. Based on the Raman spectroscopy investigations, an increase of the unit cell volume was accompanied by a decrease in the octahedra distortion and the decrease in their tilt angle, which led to the increase in the symmetry of the structure [51, 52]. According to TG-measurements, a higher unit cell volume was responsible for better water uptake during hydration up to 1.5 mol H_2O per formula unit [50]. Analysis of IR-spectra confirmed that proton form in the structure was OH-groups, including H-bonds with different strengths [50]. $BaLa_{0.9}Ba_{0.1}InO_{3.95}$ was identified as the most conductive composition among acceptor- and donor-doped materials.

An increase in the unit cell volume can be obtained not only by the dopant radius term, but also by the dopant concentration term. The acceptor-doped $Ba_{1+x}La_{1-x}InO_{4-0.5x}$ ($0 \le x \le 0.15$) [44] and donor-doped $BaLaIn_{1-x}Ti_xO_{4+0.5x}$ ($0 \le x \le 0.15$) [46], $BaLaIn_{1-x}Nb_xO_{4+x}$ ($0 \le x \le 0.10$) [49] solid solutions were obtained. An increase in the dopant concentration led to an increase in both the unit cell volume and the proton concentration in the structure. However, the concentration profile of proton conductivity was found to be non-monotonic.

The maximum of proton conductivity was observed for a small dopant concentration ($x = 0.05$ for Ti-doped solid solution and $x = 0.1$ for Ba- and Nb- doped solid solutions) (Figure 3). Exceeding this value led to decreasing proton conductivity values due to the formation of proton-aggregating clusters:

$$M_A' + (OH)_o^{\bullet} \rightarrow (M_A' \cdot (OH)_o^{\bullet})^{\times} \quad (4)$$

$$M_B^{\bullet} + (OH)_i' \rightarrow (M_B^{\bullet} \cdot (OH)_i')^{\times} \quad (5)$$

Consequently, a combination of optimal concentration of dopant and its size is necessary for the design of the most conductive proton-conducting electrolytes with layered perovskite structures. It should be noted that all acceptor- and donor-doped samples based on $BaLaInO_4$ exhibit ~ 90–98% proton conductivity in wet air below 400 °C.

Figure 3, where the temperature dependencies of proton conductivity for the different layered perovskites $AA'BO_4$ are presented, shows that the most conductive composition is the sample $BaNd_{0.8}Ca_{0.2}InO_{3.9}$. However, the proton transport numbers for this composition do not exceed 0.57 at low temperatures (250–475 °C). At the same time, the $BaLa_{0.9}Ba_{0.1}InO_{3.95}$ composition is characterized by almost fully proton conductivity (95–98% below 400 °C [43]) despite slightly lower proton conductivity values.

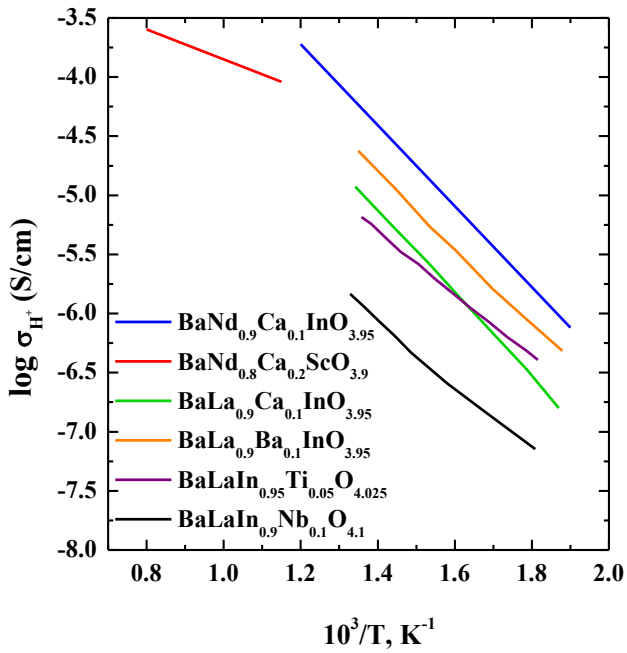

Figure 3 The temperature dependencies of proton conductivity for doped compositions based on $BaNdInO_4$ [40], $BaNdScO_4$ [41], $SrLaInO_4$ [42], $BaLaInO_4$ [43, 44, 49].

3. Hexagonal perovskites

3.1. $Ba_7Nb_4MoO_{20}$

The discovery of oxygen-ion conductivity in a hexagonal perovskite by Fop et al. in 2016 [55] has prompted extensive research on this structural type. The structure of hexagonal perovskites has long been defined. If the ABO_3 perovskite structure generally consists of corner-sharing BO_6 octahedral units, then, with a significant difference in size between the constituent cations, some of the BO_6 octahedra share faces, forming hexagonal polytypes. Mixed combinations of corner-sharing and face-sharing octahedra can lead to a variety of hexagonal perovskite derivatives, which are able to accommodate cationic and anionic vacancies [56, 57].

Although the phase $Ba_3MoNbO_{8.5}$ (intergrowth structure between the 9R perovskite and palmierite structures) did not show a high conductivity, another $Ba_7Nb_4MoO_{20}$ composition was found to be a more promising ionic conductor. A single-phase $Ba_7Nb_4MoO_{20}$ material can be obtained by the conventional solid-state reaction at 1050 °C for 48 h. The $Ba_7Nb_4MoO_{20}$ phase exhibits a cation deficient hexagonal perovskite structure with the unusual polytype 7H *(hhchhcc)*. It crystallizes in the *P*3*m*1 space group with the hexagonal lattice parameters of a = 5.8644(2) Å and c = 16.5272(4) Å. The unit cell of $Ba_7Nb_4MoO_{20}$ can be considered as an ordered intergrowth along the *c*-axis of the structural units corresponding to the 12R and the palmierite polytypes. Both types of blocks are isolated through the cationic vacancies, forming a layered structure. The existence of two cationic empty sites per unit cell is a possible reason for adopting the 7H polytype containing two *hh* pairs[58]. According to [58], the short O1–O2 distance (~2.0 Å) does not allow for simultaneous occupation of two oxygen sites. The O1 and O2 sites are therefore partially occupied, leading to mixed four-, five- and six-fold local coordinates of the d-metal atoms (M1) along the palmierite-like layers. When heated above 290 °C, a thermal reorganization of the oxygen fractional occupancies at the O1 and O2 sites occurs: the O1 fractional occupancy increases, while the fractional occupancy of O2 decreases, and above 500 °C, the O1 site is fully occupied, while O2 is empty. The partially occupied oxygen sites and the intrinsic vacancies along the palmierite-like layers provide viable oxide ion migration pathways and allow for the formation and diffusion of protonic (hydroxyl) defects forming during the dissociative water absorption.

Thermogravimetric analysis conducted in a cooling mode under humidified air (pH_2O ~0.021 atm) confirms water uptake of $Ba_7Nb_4MoO_{20}$ [59]. At room temperature, its weight increase corresponds to ~0.80 H_2O molecules per formula unit. The hydration is correlated with the change in O1–O2 occupancies. The phase of $Ba_7Nb_4MoO_{20}$ is stable under reducing conditions and after heating in pure CO_2 (1 atm) between 400 and 600 °C. Electromotive force measurements and conductivity measurements depending on oxygen partial pressure (pO_2) variation indicate that the undoped $Ba_7Nb_4MoO_{20}$ hexagonal perovskite is an oxygen-ionic conductor with a negligible level of electronic conductivity. At low oxygen partial pressures (10^{-18}–10^{-16} atm at 600–800 °C), *n*-type electronic conductivity is observed. In wet air (pH_2O ~0.021 atm), an increase in conductivity is attributed to proton conductivity, and the proton conductivity value is comparable with the one observed for $BaCe_{0.9}Y_{0.1}O_{3-\delta}$. The calculated proton transport number reaches ~0.80 at 525 °C. The activation energy of proton bulk conductivity is 0.57 ± 0.04 eV. The authors of the study [59] believe that isolated lower coordination moieties (tetrahedral) provide more dynamic environments for oxygen migration; therefore, the presence of a flexible average tetrahedral environment facilitates proton mobility. This is the reason why the $Ba_3NbMoO_{8.5}$ structural analog (intergrowth of palmierite layers and 9R perovskite blocks), containing predominantly higher coordination geometries in the palmierite layer, does not exhibit proton conductivity.

Oxygen-ionic conduction in a nonstoichiometric $Ba_7Nb_{3.9}Mo_{1.1}O_{20.05}$ compound was described by Yashima in 2021 [60]. It was shown that the bulk conductivity of $Ba_7Nb_{3.9}Mo_{1.1}O_{20.05}$ was remarkably high (5.8×10^{-4} S cm^{-1} at 310 °C), exceeding the values for Bi_2O_3- and zirconia-based materials. The high conductivity of $Ba_7Nb_{3.9}Mo_{1.1}O_{20.05}$ was attributed to the interstitial oxygen.

Thus, phases based on the $Ba_7Nb_4MoO_{20}$ hexagonal perovskite are exceptional candidates for application as a dual-ion solid state electrolyte in a ceramic fuel cell, which will combine the advantages of both oxide ion and proton-conducting electrolytes.

3.2. $Ba_5Er_2Al_2ZrO_{13}$

Among hexagonal perovskite-related oxides, the formation of intergrowth structures can occur with oxygen-deficient fragments of different structures [61]. For example, the composition of $Ba_5Er_2Al_2ZrO_{13}$ adopts a hexagonal perovskite-related structure consisting of triple-layer cubic perovskite blocks, which are separated by an oxygen-deficient hexagonal $BaO(V_o)$-layer [62]. The lattice parameters of the $Ba_5Er_2Al_2ZrO_{13}$phase were obtained as a = 5.9629(3) Å and c = 24.7340(1) Å

(*P*63/*mmc*). The presence of oxygen-deficient layers in the hexagonal perovskite oxides is a key condition for the appearance of high proton conductivity. This phase was first described in 2020 as a new class of proton conductors [63]. Incorporation of protons led to the formation of the phase with $Ba_5Er_2Al_2ZrO_{13.23}H_{0.46}$ composition. The proton conductivity of $Ba_5Er_2Al_2ZrO_{13}$ was higher than 10^{-3} S·cm^{-1} above 300 °C, which is comparable to the numbers reported for the best proton conductors and $Ba_7Nb_4MoO_{20}$.

3.3. $Ba_5In_2Al_2ZrO_{13}$

The structure of another hexagonal perovskite composition, $Ba_5In_2Al_2ZrO_{13}$, was described by Shpanchenko et al. [63]. It can be seen as a result of the intergrowth of Ba_2InAlO_5-like blocks and $BaZrO_3$-blocks along the *c*-axis. Two 4f positions are occupied by In- and Al-atoms; and oxygen atoms and vacancies in BaO_2–layers are disordered (Figure 4).

The possibility of proton transport in this compound was revealed for the first time in 2022 [64]. It was found that the compositions of $Ba_5Er_2Al_2ZrO_{13}$ and $Ba_5Er_2Al_2ZrO_{13}$ had close hydration degrees (~0.3 mol per formula unit). The presence of different types of OH^--groups in the structure of hydrated $Ba_5In_2Al_2ZrO_{12.7}(OH)_{0.6}$ phase was confirmed by IR-analysis and caused by their participation in different hydrogen bonds.

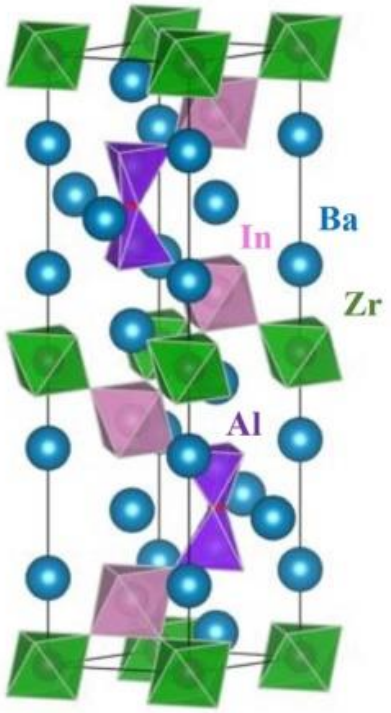

Figure 4 Crystal structure of $Ba_5In_2Al_2ZrO_{13}$.

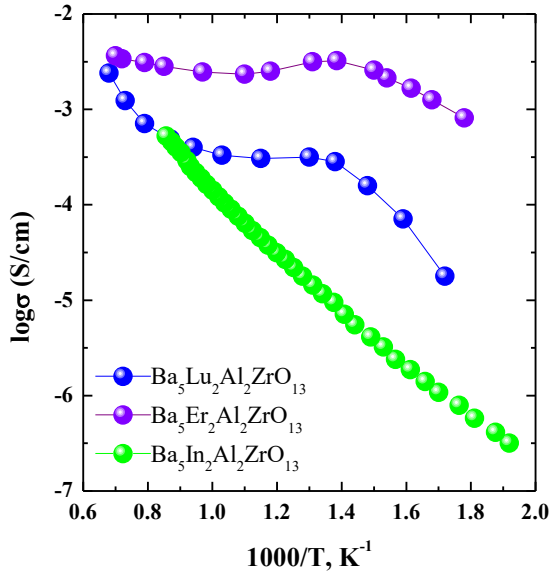

Figure 5 Temperature dependencies of total conductivity for $Ba_5Er_2Al_2ZrO_{13}$ [62], $Ba_5Lu_2Al_2ZrO_{13}$ [62] and $Ba_5In_2Al_2ZrO_{13}$ [64] in wet air (pH_2O = 1.92·10^{-2} atm).

Figure 5 presents the temperature dependencies of total conductivity in wet air for several hexagonal perovskites, including $Ba_5Er_2Al_2ZrO_{13}$ [62], $Ba_5Lu_2Al_2ZrO_{13}$ [62] and $Ba_5In_2Al_2ZrO_{13}$ [64]. The Er-containing sample exhibits the highest conductivity among others. The possible reason for this is the implementation of the optimal migration volume for proton transport.

4. Conclusions

The layered and hexagonal perovskites are relatively new and promising classes of protonic conductors. Various type of doping can significantly improve their transport properties, including conductivity values and ionic transport numbers. However, the further research is needed to obtain compositions with suitable characteristics for their actual application as electrolyte materials in SOFCs. We believe that novel ceramic materials with layered and hexagonal perovskite structures will be developed, and they will be suitable for use in energy conversion devices.

Supplementary materials

No supplementary materials are available.

Funding

This work was supported by the Russian Science Foundation (grant no 22-79-10003).

Russian Science Foundation

Acknowledgments

None.

Author contributions

Conceptualization: N.T., I.A.
Funding acquisition: A.G., N.T., I.A.
Methodology: A.G., N.T., I.A. , D.M.
Visualization: N.T., A.G.
Writing – original draft: N.T., I.A, D.M.
Writing – review & editing: N.T., I.A., D.M.

Conflict of interest

The authors declare no conflict of interest.

Additional information

Institute's website:

Institute of High Temperature Electrochemistry UB RAS, http://www.ihte.uran.ru/

Institute of High Temperature Electrochemistry of the Ural Branch of the Russian Academy of Sciences IHTE

References

1. Filippov SP, Yaroslavtsev AB, Hydrogen energy: development prospects and materials, Russ. Chem. Rev. **90(6)** (2021) 627-643. https://doi.org/10.1070/RCR5014

2. Istomin SYa, Lyskov NV, Mazo GN, Antipov EV, Electrode materials based on complex d-metal oxides for symmetrical solid oxide fuel cells, Russ. Chem. Rev. **90(6)** (2021) 644-676. https://doi.org/10.1070/RCR4979

3. Nikonov AV, Pavzderin NB, Khrustov VR, Properties of the La0.6Sr0.4Co0.8Fe0.2O3−δ – Ce0.73Gd0.27O2−δ Composite Cathode Formed from Nanopowders, Russ. J. Electrochem. **58** (2022) 311-320. https://doi.org/10.1134/S1023193522040103

4. Voloshin BV, Koshevoi EI, Ulihin AS, Popov MP, et al., Modifying the La0.6Sr0.4Co0.2Fe0.8O3−δ Cathodic Material by Ferroactive Molybdenum Cation, Russ. J. Electrochem. **58** (2022) 163-167. https://doi.org/10.1134/S1023193522020112

5. Nefedkin SI, Ivanenko AV, Pavlov VI, Panov SV, et al., Hydrogen–Air Fuel Cells with Open Cathode for High-Rate Electric Energy Systems, Russ. J. Electrochem. **58** (2022) 151-162. https://doi.org/10.1134/S1023193522020082

6. Ivanov AI, Bredikhin SI, Kharton VV, Mixed Ionic-Electronic Conductivity of the Fluorite-Type Ce1−x−yLaxPryO2−δ Solid Solutions under Reducing Conditions, Russ. J. Electrochem. **58** (2022) 122-130. https://doi.org/10.1134/S1023193522020045

7. Agarkova EA, Zadorozhnaya OYu, Burmistrov IN, Agarkov DA, et al., Tape Casting of Bilayered Anode Supports and Electrochemical Performance of SOFCs Based on Them, Russ. J. Electrochem. **58** (2022) 114-121. https://doi.org/10.1134/S1023193522020033

8. Voloshin BV, Bulina NV, Popov MP, Nemudry AP, Operando X-Ray Diffraction Analysis of a Microtubular La0.6Sr0.4Co0.2Fe0.8O3−δ Membrane, Russ. J. Electrochem. **58** (2022) 100-104. https://doi.org/10.1134/S1023193522020100

9. Lyskov NV, Galin MZ, Napol'skii PhS, Mazo GN, Increasing the Electrochemical Activity of the Pr1.95La0.05CuO4 Cathode by Laser Modification of the Electrode/Electrolyte Interface Profile, Russ. J. Electrochem. **58** (2022) 93-99. https://doi.org/10.1134/S1023193522020070

10. Kasyanova AV, Tarutina LR, Rudenko AO, Laygaeva JG, et al., Ba(Ce,Zr)O3-based electrodes for protonic ceramic electrochemical cells: towards highly compatible functionality and triple-conducting behavior, Russ. Chem. Rev. **86(6)** (2020) 667-692. https://doi.org/10.1070/RCR4928

11. Lomonova EE, Agarkov DA, Borik MA, Korableva GM, et al., Structure and Transport Characteristics of Single-Crystal and Ceramic ZrO2–Y2O3 Solid Electrolytes, Russ. J. Electrochem. **58** (2022) 105-113. https://doi.org/10.1134/S1023193522020069

12. Kunshina GB, Bocharova IV, Shcherbina OB, Electrical Conductivity and Mechanical Properties of Li7-3xAlxLa3Zr2O12 Solid Electrolyte, Inorg. Mater. **58** (2022) 147-153. https://doi.org/10.1134/S0020168522020091

13. Ruddlesden SN, Popper P, New compounds of the K2NiF4 type, Acta Crystallogr. **10** (1957) 538-539. https://doi.org/10.1107/S0365110X57001929

14. Page YLe, Siegrist T, Sunshine SA, Schneemeyer LF, et al., Structural properties of Ba2RCu3O7 high-Tc superconductors, Phys. Rev. B. **36** (1987) 3517-3621. https://doi.org/10.1103/PhysRevB.36.3617

15. Cheong S-W, Thompson JD, Fisk Z, Properties of La2CuO4 and related compounds, Physica C. **158** (1989) 109-126. https://doi.org/10.1016/0921-4534(89)90306-7

16. Tokura Y, Takagi H, Uchida S, A superconducting copper oxide compound with electrons as the charge carriers, Nature. **337** (1989) 345-347. https://doi.org/10.1038/337345a0

17. Hauck J, Mika K, Krabbes G, Search for new high Tc oxide structures, Physica C. **185-189** (1991) 721-722. https://doi.org/10.1016/0921-4534(91)92163-6

18. Gangily P, Rao NR, Crystal Chemistry and Magnetic Properties of Layered Metal Oxides Possessing the K2NiF4 or Related Structures, J. Solid State Chem. **53** (1984) 193-216. https://doi.org/10.1016/0022-4596(84)90094-X

19. Kawano S, Achiwa N, Kamegashira N, Aoki M, Magnetic properties of K2NiF4 type oxides, SrLaMnO4+x (0 ≤ x ≤ 0.2), J. Phys. Colloques. **49** (1988) 829-830. https://doi.org/10.1051/jphyscol:19888373

20. Moritomo Y, Tomioka Y, Asamitsu A, Tokura Y, Magnetic and electronic properties in hole-doped manganese oxides with layered structures: La1−xSr1+xMnO4, Phys. Rev. B **51** (1995)3297-3300. https://doi.org/10.1103/PhysRevB.51.3297

21. Hector AL, Knee CS, MacDonald AI, Price DJ, et al., An unusual magnetic structure in Sr2FeO3F and magnetic structures of K2NiF4-type iron (III) oxides and oxide halides,

including the cobalt substituted series Sr2Fe1−xCoxO3Cl, J. Mater. Chem. **15** (2005) 3093–3103. https://doi.org/10.1039/B505617A

22. Amow G, Davidson IJ, Skinner SJ, A comparative study of the Ruddlesden-Popper series, Lan+1NinO3n+1 (n=1, 2 and 3), for solid-oxide fuel-cell cathode applications, Solid State Ion. **177** (2006) 1205–1210. https://doi.org/10.1016/j.ssi.2006.05.005

23. Amow G, Skinner SJ, Recent developments in Ruddlesden–Popper nickelate systems for solid oxide fuel cell cathodes, J. Solid State Electrochem. **10** (2006) 538–546. https://doi.org/10.1007/s10008-006-0127-x

24. Sayers R, Liu J, Rustumji B, Skinner SJ, Novel K2NiF4-Type Materials for Solid Oxide Fuel Cells: Compatibility with Electrolytes in the Intermediate Temperature Range, Fuel Cell. **08** (2008) 338–343. https://doi.org/10.1002/fuce.200800023

25. Takahashi S, Nishimoto S, Matsuda M, Miyake M, Electrode Properties of the Ruddlesden–Popper Series, Lan+1NinO3n+1 (n = 1, 2 and 3), as Intermediate-Temperature Solid Oxide Fuel Cells, J. Am. Ceram. Soc. **93** (2010) 2329–2333. https://doi.org/10.1111/j.1551-2916.2010.03743.x

26. Montenegro-Hernandez A, Vega-Castillo J, Mogni L, Caneiro A, Thermal stability of Ln2NiO4+δ (Ln: La, Pr, Nd) and their chemical compatibility with YSZ and CGO solid electrolytes, Int. J. Hydrog. Energy. **36(24)** (2011) 15704-15714. https://doi.org/10.1016/j.ijhydene.2011.08.105

27. Grimaud A, Mauvy F, Bassat JM, Fourcade S, et al., Hydration and transport properties of the Pr2-xSrxNiO4+δ compounds as H+-SOFC cathodes, J. Mater. Chem. **22** (2012) 16017-16025. https://doi.org/10.1039/C2JM31812A

28. Ferkhi M, Ahmed Yahia H, Electrochemical and morphological characterizations of La2-xNiO4+δ (x = 0.01, 0.02, 0.03 and 0.05) as new cathodes materials for IT-SOFC, Mater. Res. Bull. **83** (2016) 268–274. https://doi.org/10.1016/j.materresbull.2016.06.009

29. Sharma RK, Burriel M, Dessemond L, Bassat JM, et al., Lan+1NinO3n+1 (n = 2 and 3) phases and composites for solid oxide fuel cell cathodes: Facile synthesis and electrochemical properties, J. Power Sources. **325** (2016) 337-345. https://doi.org/10.1016/j.jpowsour.2016.06.047

30. Vibhu V, Rougier A, Nicollet C, Flura A, et al., Pr4Ni3O10+δ: A new promising oxygen electrode material for solid oxide fuel cells, J. Power Sources. **317** (2016) 184-193. https://doi.org/10.1016/j.jpowsour.2016.03.012

31. Yatoo MA, Du Z, Zhao H, Aguadero A, et al., La2Pr2Ni3O10±δ Ruddlesden-Popper phase as potential intermediate temperature-solid oxide fuel cell cathodes, Solid State Ion. **320** (2018) 148–151. https://doi.org/10.1016/j.ssi.2018.02.043

32. Morales-Zapata MA, Larrea A, Laguna-Bercero MA, Reversible operation performance of microtubular solid oxide cells with a nickelate-based oxygen electrode, Int. J. Hydrog. Energy. **45(8)** (2020) 5535-5542. https://doi.org/10.1016/j.ijhydene.2019.05.122

33. Danielson E, Devenney M, Giaquinta DM, Golden JH, et al., X-ray powder structure of Sr2CeO4: A new luminescent material discovered by combinatorial chemistry, J. Mol. Struct. **470** (1998) 229-235. https://doi.org/10.1016/S0022-2860(98)00485-2

34. Li J, Li X, Hu S, Li Y, et al., Photoluminescence mechanisms of color-tunable Sr2CeO4: Eu3+, Dy3+ phosphors based on experimental and first-principles investigation, Opt. Mater. **35(12)** (2013) 2309-2313. https://doi.org/10.1016/j.optmat.2013.06.024

35. Sahu M, Gupta SK, Jain D, Saxena MK, et al., Solid state speciation of uranium and its local structure in Sr2CeO4 using photoluminescence spectroscopy, Spectrochim. Acta A. **195** (2018) 113-119. https://doi.org/10.1016/j.saa.2018.01.048

36. Jia Y, Shen S, Wang D, Wang X, et al., Composite Sr2TiO4/SrTiO3(La,Cr) heterojunction based photocatalyst for hydrogen production under visible light irradiation, J. Mater. Chem. A. **1** (2013) 7905–7912. https://doi.org/10.1039/c3ta11326d

37. Zhang H, Ni S, Mi Y, Xu X, Ruddlesden-Popper compound Sr2TiO4 co-doped with La and Fe for efficient photocatalytic hydrogen production, J. Catal. **359** (2018) 112-121. https://doi.org/10.1016/j.jcat.2017.12.031

38. Ziati M, Bekkioui N, Ez-Zahraouy H, Ruddlesden-Popper compound Sr2TiO4 doped with chalcogens for optoelectronic applications: Insights from first-principle calculations, J. Chem. Phys. **548** (2021) 111221. https://doi.org/10.1016/j.chemphys.2021.111221

39. Tarasova N, Animitsa I, Protonic transport in oxyfluorides Ba2InO3F and Ba3In2O5F2 with Ruddlesden-Popper structure, Solid State Ion. **275** (2015) 53–57. https://doi.org/10.1016/j.ssi.2015.03.025

40. Zhou Y, Shiraiwa M, Nagao M, Fujii K, et al., Protonic Conduction in the BaNdInO4 Structure Achieved by Acceptor Doping, Chem. Mater. **33** (2021) 2139 - 2146. https://doi.org/10.1021/acs.chemmater.0c04828

41. Shiraiwa M, Kido T, Fujii K, Yashima M, High-temperature proton conductors based on the (110) layered perovskite BaNdScO4, J. Mat. Chem. A. **9** (2021) 8607. https://doi.org/10.1039/D0TA11573H

42. Troncoso L, Arce MD, Fernandez-Diaz MT, Mogni LV, et al., Water insertion and combined interstitial-vacancy oxygen conduction in the layered perovskites La1.2Sr0.8-xBaxInO4+d, New J. Chem. **43** (2019) 6087. https://doi.org/10.1039/C8NJ05320K

43. Tarasova N, Animitsa I, Galisheva A, Korona D, Incorporation and Conduction of Protons in Ca, Sr, Ba-Doped BaLaInO4 with Ruddlesden-Popper Structure, Materials. **12** (2019) 1668. https://doi.org/10.3390/ma12101668

44. Tarasova N, Animitsa I, Galisheva A, Pryakhina V, Protonic transport in the new phases BaLaIn0.9M0.1O4.05 (M=Ti, Zr) with Ruddlesden-Popper structure, Solid State Sci. **101** (2020) 106121. https://doi.org/10.1016/j.solidstatesciences.2020.106121

45. Tarasova N, Animitsa I, Galisheva A, Electrical properties of new protonic conductors Ba1+xLa1−xInO4−0.5x with Ruddlesden-Popper structure, J. Solid State Electrochem. **24** (2020) 1497-1508. https://doi.org/10.1007/s10008-020-04630-1

46. Tarasova N, Galisheva A, Animitsa I, Improvement of oxygen-ionic and protonic conductivity of BaLaInO4 through Ti doping, Ionics. **26** (2020) 5075-5088. https://doi.org/10.1007/s11581-020-03659-6

47. Tarasova N, Galisheva A, Animitsa I, Ba2+/Ti4+-co-doped layered perovskite B a LaInO4: the structure and ionic (O2−, H+) conductivity, Int. J. Hydrog. Energy **46(32)**

(2021) 16868-16877. https://doi.org/10.1016/j.ijhydene.2021.02.044

48. Tarasova N, Galisheva A, Animitsa I, Korona D, Hydration and the State of Oxygen–Hydrogen Groups in the Complex Oxide BaLaIn0.9Nb0.1O4.1 with the Ruddlesden–Popper Structure, Russian J. Phys. Chem. A. **94** (2020) 818-821. https://doi.org/10.1134/S0036024420030309

49. Tarasova N, Galisheva A, Animitsa I, Dmitrieva A, The Effect of Donor Doping on the Ionic (O2–, H+) Transport in Novel Complex Oxides BaLaIn1– xNbxO4+x with the Ruddlesden–Popper Structure, Russian J. Electrochem. **57** (2021) 962-969. https://doi.org/10.1134/S1023193521080115

50. Tarasova N, Animitsa I, Galisheva A Effect of acceptor and donor doping on the state of protons in block-layered structures based on BaLaInO4, Solid State Commun. **323** (2021) 14093. https://doi.org/10.1016/j.ssc.2020.114093

51. Tarasova N, Animitsa I, Galisheva A, Effect of doping on the local structure of new block-layered proton conductors based on BaLaInO4, J. Raman Spectrosc. **51** (2020) 2290-2297. https://doi.org/10.1002/jrs.5966

52. Tarasova N, Animitsa I, Galisheva A, Spectroscopic and transport properties of Ba- and Ti-doped BaLaInO4, J. Raman Spectrosc. **52** (2021) 980-987. https://doi.org/10.1002/jrs.6078

53. Kreuer K, Proton-Conducting Oxides, Ann. Rev. Mater. Res. **33** (2003) 333-359. https://doi.org/10.1146/annurev.matsci.33.022802.091825

54. Duan C, Huang J, Sullivan N, O'Hayre R. Proton-conducting oxides for energy conversion and storage, Applied Physics Reviews. **7** (2020) 011314. https://doi.org/10.1063/1.5135319

55. Fop S, et al., Oxide ion conductivity in the hexagonal perovskite derivative Ba3MoNbO8.5, J. Am. Chem. Soc. **138** (2016) 16764–16769. https://doi.org/10.1021/jacs.6b10730

56. Katz L, Ward R, Structure relations in mixed metal oxides, Inorg. Chem. **3** (1964) 205–211. https://doi.org/10.1021/ic50012a013

57. Darriet J, Subramanian MA, Structural relationships between compounds based on the stacking of mixed layers related to hexagonal perovskite-type structures, J. Mater. Chem. **5** (1995) 543-552. https://doi.org/10.1039/JM9950500543

58. Garcıa-Gonzalez E, Parras M, Gonzalez-Calbet JM, Crystal Structure of an Unusual Polytype:7H-Ba7Nb4MoO20, Chem. Mater. **11** (1999) 433-437. https://doi.org/10.1021/cm9810111i

59. Fop S, McCombie KS, Wildman EJ, Skakle JMS, et al., High oxide ion and proton conductivity in a disordered hexagonal perovskite, Nature Mater. **19** (2020) 752–757. https://doi.org/10.1038/s41563-020-0629-4

60. Yashima M, Tsujiguchi T, Sakuda Y, Yasui Y, et al., High oxide-ion conductivity through the interstitial oxygen site in Ba7Nb4MoO20-based hexagonal perovskite related oxides, Nature Comm. **12** (2021) 556. https://doi.org/10.1038/s41467-020-20859-w

61. Abakumov AM, Antipov EV, Kovba LM, Kopnin EM, et al., Complex oxides with coherent intergrowth structures, Russ. Chem. Rev. **64(8)** (1995) 719-729. https://doi.org/10.1070/RC1995v064n08ABEH000171

62. Murakami T, Hester JR, Yashima M, High Proton Conductivity in Ba5Er2Al2ZrO13, a Hexagonal Perovskite-Related Oxide with Intrinsically Oxygen-Deficient Layers, J. Am. Chem. Soc. **142** (2020) 11653–11657. https://doi.org/10.1021/jacs.0c02403

63. Shpanchenko R, Abakumov A, Antipov E, Kovba L, Crystal structure of Ba5In2Al2ZrO13, J. Alloy. Compd. **206** (1994) 185–188. https://doi.org/10.1016/0925-8388(94)90033-7

64. Andreev R, Korona D, Anokhina I, Animitsa I. Proton and Oxygen-Ion Conductivities of Hexagonal Perovskite Ba5In2Al2ZrO13, Materials. **15** (2022) 3944. https://doi.org/10.3390/ma15113944